

HIGH-RESOLUTION ELECTRON ENERGY-LOSS SPECTRA OF SOLID C₆₀, C₇₀ AND CARBON NANOTUBES

Ryuichi Kuzuo^a, Masami Terauchi^a, Michiyoshi Tanaka^a, Yahachi Saito^b and Hisanori Shinohara^c

^aResearch Institute for Scientific Measurements, Tohoku University, Sendai 980, Japan

^bDepartment of Electrical Engineering, Faculty of Engineering, Mie University, Tsu 514, Japan

^cDepartment of Chemistry, Faculty of Science, Nagoya University, Nagoya 464, Japan

Transmission electron energy-loss spectra of solid C₆₀, C₇₀ and carbon nanotubes have been measured. The dielectric functions have been obtained from the spectra using Kramers-Kronig analysis. The results have been compared with energy-band calculations.

1. INTRODUCTION

Since Kroto *et al.*[1] discovered new forms of carbon, "fullerenes", such as C₆₀ and C₇₀, great interest has been focused on their crystal structures[2] and electronic properties[3,4,5]. Recently, Iijima[6] discovered a new form of graphitic carbon needles, called "carbon nanotubes" or "bucky tubes", which were produced by a similar method as that to prepare the fullerenes. The present paper reports transmission electron energy-loss spectra measured from solid C₆₀, C₇₀ and carbon nanotubes and the dielectric functions obtained by Kramers-Kronig analysis (KKA) of the spectra.[7,8]. These results are compared with energy-band calculations.

2. EXPERIMENTAL

C₆₀, C₇₀ and carbon nanotubes used in the present study were produced using the d.c. arc-discharge evaporation method. Crystalline thin films of C₆₀ and C₇₀ were grown on mica substrates by evaporating in a vacuum chamber. Specimens for electron energy-loss spectroscopy (EELS) were prepared by peeling the film from the substrate and by mounting it on a specimen-supporting copper-mesh covered with a microgrid. Specimens of carbon nanotubes were prepared by dropping a droplet of alcohol containing nanotubes onto the copper-mesh.

The high-resolution electron energy-loss spectroscopy microscope used was developed as a pro-

ject of Joint Research with Industry by the Ministry of Education, Science and Culture of Japan[9,10,11]. The instrument is equipped with two Wien filters as the monochromator and the analyzer. The best values of the full widths at the half maximum (FWHM) of the zero-loss peak, or the energy resolution at present are 15meV and 30meV for cases without and with a specimen, respectively. The accelerating voltage of the incident electron beam was set at 60keV. The spectra were measured from areas of 100nm in diameter with 240~720 seconds at room temperature.

3. C₆₀ and C₇₀

Fig.1 shows electron energy-loss spectra of C₆₀ and C₇₀ in an energy region of 0~12eV. The energy resolution was 0.12eV. The prominent peaks at 6.5eV for C₆₀ and 6.4eV for C₇₀ (indicated by arrows) are caused by the $\pi \rightarrow \pi^*$ interband transitions, which are usually called the π plasmon peaks. Four and three peaks and/or shoulders (indicated by vertical lines) are seen in the spectra of C₆₀ and C₇₀, respectively. These peaks are attributed to $\pi \rightarrow \pi^*$ interband transitions. The peaks in the spectrum of C₇₀ are broader than those of C₆₀. The broadening of the peaks in C₇₀ can be attributed to the removal of the degeneracies of the π electron energy states due to a lower symmetry of C₇₀ than that of C₆₀.

Fig.2 shows the imaginary parts (ϵ_2) of the dielectric function of C₆₀ and C₇₀. They were

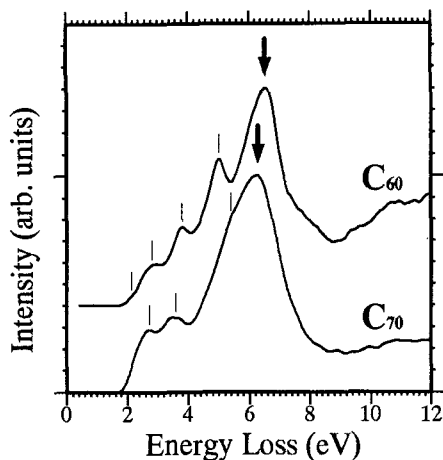


Figure 1: Electron energy-loss spectra of C_{60} and C_{70} .

derived by KKA from the loss-functions of C_{60} and C_{70} . The peaks at about 2~7eV are assigned to $\pi \rightarrow \pi^*$ interband transitions and the broad peaks above 9eV are assigned to $\sigma \rightarrow \sigma^*$, $\sigma \rightarrow \pi^*$ and $\pi \rightarrow \sigma^*$ interband transitions. According to the energy-band structure of C_{60} calculated by Saito and Oshiyama,[12] the peaks at 2.8, 3.6, 4.5 and 5.6eV in C_{60} (indicated by vertical lines) can be assigned to four $\pi \rightarrow \pi^*$ interband transitions, $h_u \rightarrow t_{1g}$, $h_g \rightarrow t_{1u}$, $h_u \rightarrow h_g$ and $g_g, h_g \rightarrow t_{2u}$, respectively.

The onset energy of the $\pi \rightarrow \pi^*$ transitions at 1.7eV in C_{60} (indicated by an arrow) is assigned to the smallest single electron excitations (band gap) from the highest occupied molecular orbitals (HOMO) to the lowest unoccupied molecular orbitals (LUMO). Since HOMO (h_u) and LUMO (t_{1u}) have the same symmetry, the transition is optically forbidden. The present experiment, however, was detectable the band gap, because multipole transitions were included on account of the use of a wide correction angle (5mrad) aperture. A band-gap energy of 1.7eV obtained is very close to a calculated direct band-gap of 1.5eV at the Brillouin zone boundary (X-point).[12]

The band-gap energy of C_{70} is 1.8eV (indicated by an arrow). This value also shows good agreement with a band-gap energy of 1.65eV calculated by Saito and Oshiyama.[13]

Fig.3 shows electron energy-loss spectra of C_{60} and C_{70} in an energy range of the carbon K-

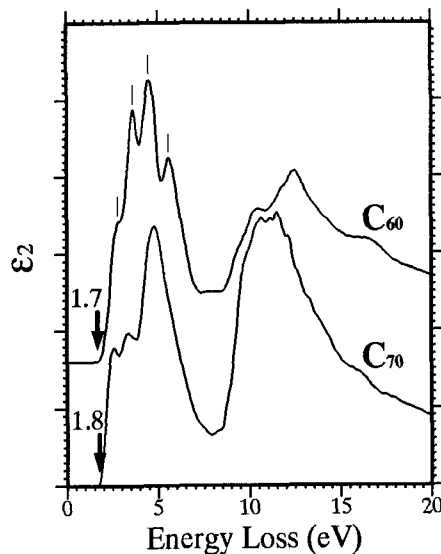


Figure 2: The imaginary parts (ϵ_2) of the dielectric function of C_{60} and C_{70} .

absorption edge. The energy resolution was 0.17eV. The structure observed between 284 eV and 290eV corresponds to $1s \rightarrow \pi^*$ transitions and that observed above 290.5eV to $1s \rightarrow \sigma^*$ transitions. In the case of C_{60} , four peaks at 284.9, 286.2, 286.7 and 288.8eV (indicated by vertical lines) can be assigned to four π^* orbitals, t_{1u} , t_{1g} , t_{2u}/h_g and g_g , respectively. In the case of C_{70} , four peaks and/or shoulders are seen at 284.8, 285.6, 286.8 and 289.4eV (indicated by vertical lines). The relative energy positions show good agreement with the inverse photoemission spectra obtained by Jost *et al.*[14]

4. CARBON NANOTUBES

Fig.4 shows an electron energy-loss spectrum of a carbon nanotube in an energy region of 0~40eV. The energy resolution was 0.31eV. The spectrum of graphite is also shown for comparison, which was measured with an electron incidence parallel to the c axis. Two distinct peaks at 6.4eV and 22.6eV (indicated by arrows) for the nanotube are identified as the π plasmon and the $\pi + \sigma$ plasmon, respectively. The energy of the $\pi + \sigma$ plasmon peak is lower than that of graphite (27.0eV) by about 5eV. The plasmon energy of graphite measured with an electron incidence perpendicular to

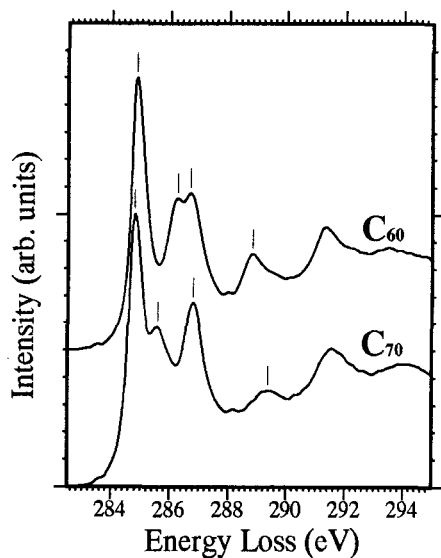


Figure 3: Carbon K-absorption edges for C_{60} and C_{70} .

the c axis is about 20eV, which is 7eV smaller than that measured with an incidence parallel to the c axis. Since the graphitic sheets of the carbon nanotube form cylinders, they are illuminated by incident electrons with both the parallel and perpendicular settings at the same time. Therefore, the plasmon energy of the carbon nanotube should be compared with the mean value of those measured at the two settings of graphite. A mean value of about 23.5eV can account for the $\pi + \sigma$ plasmon energy of the carbon nanotube.

Fig.5 shows the ϵ_2 curve of the carbon nanotube, which was derived from Fig.4 by KKA. The ϵ_2 of graphite is also shown for comparison. The peak at 4eV in ϵ_2 of the carbon nanotube is assigned to $\pi \rightarrow \pi^*$ interband transitions, and the broad peak at 12~14eV is assigned to $\sigma \rightarrow \sigma^*$, $\sigma \rightarrow \pi^*$ and $\pi \rightarrow \sigma^*$ interband transitions by consulting the results for graphite. The peak is much broader than that of graphite. This can be attributed to the removal of the degeneracies of the π electron energy states due to the curving of graphitic sheets in the nanotube. The ϵ_2 curve of the nanotube in the low-energy region shows a behavior like an insulator. However, whether the nanotube is an insulator or not cannot be determined from the curve, because the ϵ_2 in a region from 0 to 3eV is not accurate enough owing to

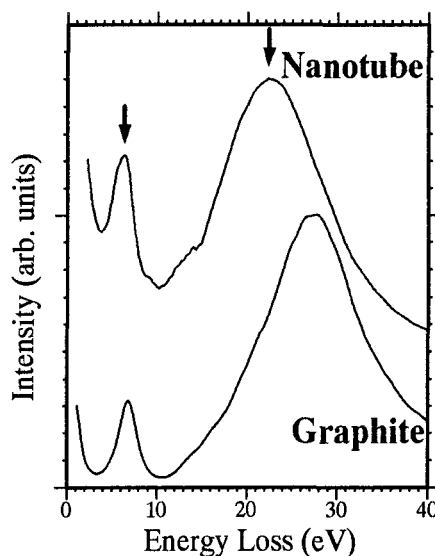


Figure 4: Electron energy-loss spectra of the carbon nanotube and graphite.

errors introduced at the subtraction of zero-loss intensity from the raw data by a Lorentz fit.

Fig.6 shows electron energy-loss spectra of the carbon nanotube and graphite in an energy region of the carbon K-absorption edge. The energy resolution was 0.38eV. The spectrum of the nanotube is similar to that of graphite; transitions from $1s$ to the unoccupied π^* levels and to the unoccupied σ^* levels are seen at 285.5eV and 292eV, respectively, in both figures. The fact that the $1s \rightarrow \pi^*$ transition peak of the carbon nanotube is slightly broader than that of graphite can again be explained by the removal of the degeneracies of the π^* states in the curved graphitic sheets.

We have measured energy-loss spectra of eight carbon nanotubes. Carbon nanotubes which have diameters larger than about 20nm showed a π plasmon peak at 6.4eV with a shoulder at 5.2eV. Carbon nanotubes which have diameters smaller than about 20nm showed a π plasmon peak at 5.2eV with a shoulder at 6.4eV. These results suggest that the π plasmon energy or the energies of π and π^* states depends on the diameter of the nanotube. On the other hand, the $\pi + \sigma$ plasmon energies of all the nanotubes examined ranged from 22.0 to 24.5eV. No special relation was found between the values of the $\pi + \sigma$ plas-

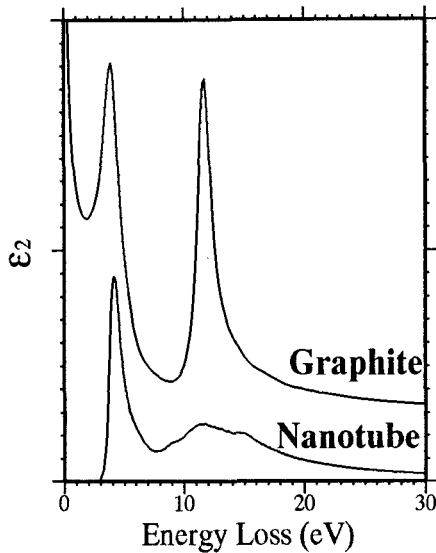


Figure 5: The imaginary parts (ϵ_2) of the dielectric function of the carbon nanotube and graphite.

mon and the diameters of the nanotubes.

REFERENCES

1. H. W. Kroto, J. R. Heath, S. C. O'Brien, R. F. Curl and R. E. Smalley : *Nature*, **318** (1985) 162.
2. R. M. Fleming, T. Siegrist, P. Marsh, B. Hessen, A. R. Kortan, D. W. Murphy, R. C. Haddon, R. Tycko, G. Dabbagh, A. M. Muijsce, M. L. Kaplan and S. M. Zahurak : *Mater. Res. Soc. Symp. Proc.*, **206** (1991) 691.
3. A. F. Hebard, M. J. Rosseinsky, R. C. Haddon, D. W. Murphy, S. H. Glarum, T. M. Palstra, A. P. Ramirez and A. R. Kortan : *Nature*, **350** (1991) 60.
4. M. J. Rosseinsky, A. P. Ramirez, S. H. Glarum, D. W. Murphy, R. C. Haddon, A. F. Hebard, T. M. Palstra, A. R. Kortan, S. M. Zahurak and A. V. Makhija : *Phys. Rev. Lett.*, **66** (1991) 2830.
5. K. Holczer, O. Klein, S. M. Huang, R. B. Kaner, K. J. Fu, R. L. Whetten and F. Diederich : *Science*, **252** (1991) 1154.
6. S. Iijima : *Nature*, **354** (1991) 56.
7. R. Kuzuo, M. Terauchi, M. Tanaka, Y. Saito and H. Shinohara : *Jpn. J. Appl. Phys.*, **30** (1991) L1817.
8. R. Kuzuo, M. Terauchi and M. Tanaka : *Jpn. J. Appl. Phys.*, **31** (1992) L1484.
9. K. Tsuno, M. Terauchi and M. Tanaka : *Optik*, **83** (1988) 77.
10. M. Terauchi, R. Kuzuo, F. Satou, M. Tanaka, K. Tsuno and J. Ohyama : *Proc. Int. Congress for Electron Microscopy* (San Francisco Press, San Francisco, 1990).
11. M. Terauchi, R. Kuzuo, F. Satou, M. Tanaka, K. Tsuno and J. Ohyama : *Microsc. Microanal. Microstruct.*, **2** (1991) 351.
12. S. Saito and A. Oshiyama : *Phys. Rev. Lett.*, **66** (1991) 2637.
13. S. Saito and A. Oshiyama : *Phys. Rev. B.*, **44** (1991) 11532.
14. M. B. Jost, P. J. Benning, D. M. Poirier, J. H. Weaver, L. P. F. Chibante and R. E. Smalley : *Chem. Phys. Lett.*, **184** (1991) 423.

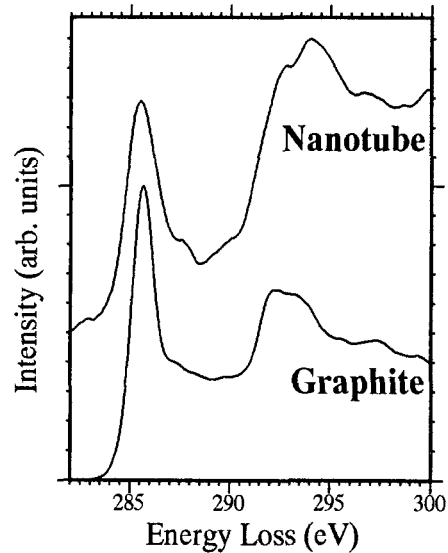


Figure 6: Carbon K-absorption edges for the carbon nanotube and graphite.